Received 6 August 2020; revised 26 August 2020; accepted 26 August 2020. Date of publication 8 September 2020; date of current version 6 October 2020.
The review of this article was arranged by Editor M. Chan.

Digital Object Identifier 10.1109/JEDS.2020.3022571

Low Turn-Off Loss 4H-SiC Insulated Gate Bipolar Transistor With a Trench Heterojunction Collector

YING WANG [1] (Senior Member, IEEE), CHENG-HAO YU [1], HONG-KAI MAO [1], XUE WU [2], FANG-WEN SU [1], XING-JI LI [3] (Senior Member, IEEE), AND JIAN-QUN YANG [3] (Member, IEEE)

1 Key Laboratory of RF Circuits and Systems, Ministry of Education, Hangzhou Dianzi University, Hangzhou 310018, China
2 National Key Laboratory of Analog Integrated Circuits, China Electronics Technology Group Corporation, Chongqin 400060, China
3 National Key Laboratory of Materials Behavior and Evaluation Technology in Space Environment, Harbin Institute of Technology, Harbin 150080, China

CORRESPONDING AUTHORS: Y. WANG AND X.-J. LI (e-mail: wangying7711@yahoo.com; lxj0218@hit.edu.cn)

This work was supported in part by the National Natural Science Foundation of China under Grant 61774052 and Grant 61904044, and in part by Science and Technology on Analog Integrated Circuit Laboratory under Grant 6142802180507.

ABSTRACT In this work, an improved 4H-SiC insulated gate bipolar transistor (IGBT), or CTH-IGBT, with a trench p-polySi/p-SiC heterojunction on the backside of the device is proposed to reduce the turn-off energy loss (E_{off}) and turn-off time (T_{off}). The electrical properties of the proposed and contrast structures are all simulated using the ATLAS simulation software to research the working mechanism of this improved structure. For the static performance, the specific ON-resistance ($R_{on,sp}$) and the figure of merit (FOM $= V_{BR}^2/R_{on,sp}$) are not influenced much as compared to the traditional structure at the same breakdown voltage (V_{BR}) of 12 kV. However, with a prominent electron current path formed by the heterojunction region of CTH-IGBT, a very available conduction path to discharge the electrons during turn-off process is proved in this article. The simulation results demonstrate that compared with the traditional structure, the turn-off energy loss of the CTH-IGBT is reduced by 76.4%, while the turn-off time is reduced by 85.0%.

INDEX TERMS 4H-SiC, heterojunction, insulated gate bipolar transistor (IGBT), turn-off loss, turn-off time, breakdown voltage.

I. INTRODUCTION

The performance of silicon-based devices is gradually approaching its limits, and it has become increasingly difficult to meet the application requirements of modern power electronic systems. The third-generation semiconductor material silicon carbide (SiC) has gradually replaced the use of silicon (Si) in power applications due to its wide band gap, high breakdown electric field, high thermal conductivity, high electron saturation drift speed and higher radiation resistance. It is widely used to make high-power devices for application in high temperature, high voltage, high frequency and radiation resistant operating environments and requirements [1]–[6].

In recent years, researchers have conducted extensive research on 4H-SiC insulated gate bipolar transistors (IGBTs) and have achieved great results in both theory and experiment [7]–[10]. The breakdown voltage of the device has grown from 6.5 kV to 27 kV [11]–[17]. However, it is found that the previous studies have mainly focused on the trade-off between the breakdown voltage and ON-resistance, while the dynamic switching characteristics of the device are ignored. In order to reduce the turn-off energy loss (E_{off}) while not substantially affecting the static performance, the use of a heterojunction structure is gradually being incorporated into the design of IGBT structures. For example, Henning *et al.* studied the electrical properties of Si/SiC and found that the barrier height of the polysilicon/4H-SiC interface may be controlled by varying polysilicon doping type [18]. Kudoh and Asano proposed a structure that had a p+-SiGe collector layer at the backside of the device [19], and Liang *et al.* analyzed the influence of interface state on the electrical properties of Si/SiC [20].

In order to further reduce the turn-off energy loss, without sacrificing the static characteristics, we have proposed the collector trench heterojunction IGBT (CTH-IGBT) with a p-polySi/p-SiC trench heterojunction on the backside of

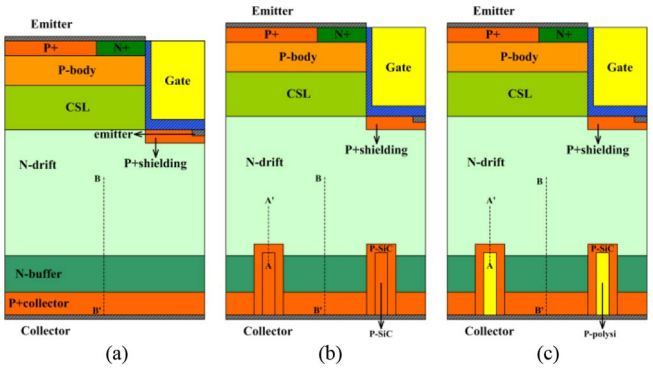

FIGURE 1. Schematic cross-sectional views of (a) C-IGBT, (b) CT-IGBT and (c) CTH-IGBT.

TABLE 1. Structural simulation parameters.

Parameters	C-IGBT	TH-IGBT
Half-cell width	2.1μm	2.1μm
N-drift thickness	160μm	170μm
Gate width	0.6μm	0.6μm
Gate depth	5μm	5μm
Trench heterojunction width	-	0.6μm
Trench heterojunction depth	-	5μm
Trench heterojunction spacing	-	0.7μm
P-SiC thickness in heterojunction	-	1.0μm
P+source doping	$5\times10^{19}cm^{-3}$	$5\times10^{19}cm^{-3}$
N+source doping	$2\times10^{19}cm^{-3}$	$2\times10^{19}cm^{-3}$
P-body doping	$4\times10^{17}cm^{-3}$	$4\times10^{17}cm^{-3}$
CSL doping	$1\times10^{15}cm^{-3}$	$1\times10^{15}cm^{-3}$
P+shielding doping	$5\times10^{18}cm^{-3}$	$5\times10^{18}cm^{-3}$
N-drift doping	$5.0\times10^{14}cm^{-3}$	$5.0\times10^{14}cm^{-3}$
N buffer doping	$1\times10^{17}cm^{-3}$	$1\times10^{17}cm^{-3}$
P+collector doping	$1\times10^{19}cm^{-3}$	$1\times10^{19}cm^{-3}$
P-polysilicon doping	-	$1\times10^{17}cm^{-3}$
P-SiC doping	-	$1\times10^{19}cm^{-3}$

the structure. The electrical characteristics of CTH-IGBT and conventional IGBT (C-IGBT) were simulated with the Silvaco ATLAS simulation software. The results show that under the same breakdown voltage of 12 kV, the turn-off energy loss of the CTH-IGBT is 76.4% lower than the C-IGBT, and the turn-off time (T_{off}) is reduced by 85.0%.

II. DEVICE STRUCTURE AND FABRICATION PROCEDURE

Fig. 1 shows the schematic cross-sectional half-cell structure views of the C-IGBT and CTH-IGBT, respectively, and the structure (b) (collector trench IGBT, CT-IGBT) is also introduced to further illustrate the role of the heterojunction. The sizes and doping concentrations of the C-IGBT and CTH-IGBT are provided in TABLE 1. In order to better compare with the previous research results, the main structural parameters of the conventional and proposed structures are identical except for the collector region below drift region [21]–[23]. At the same time, the only difference between CT-IGBT and CTH-IGBT is that the former collector trench is filled with the 4H-SiC. The thicknesses of the oxide on the bottom and sidewalls of the gate trench are 100 nm and 50 nm, respectively.

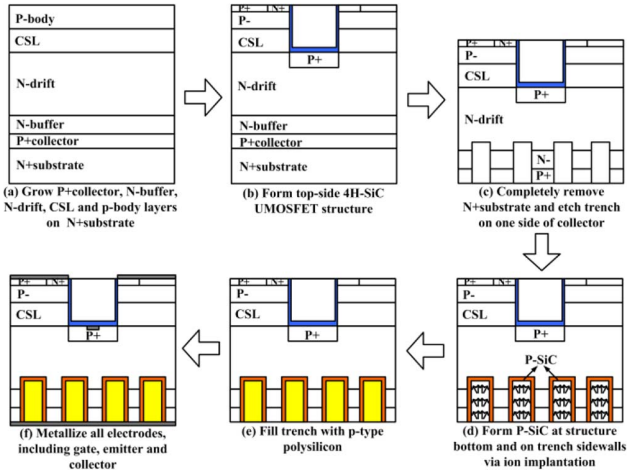

FIGURE 2. Main fabrication steps of CTH-IGBT structure.

The $I-V$, breakdown and turn-off characteristics of the structures are verified by simulations using Silvaco ATLAS software. Since the previously simulated IGBT has been manufactured and verified [24], the same material parameters and physical models for the 4H-SiC devices are introduced in this article. The key physical models include concentration-dependent mobility model (CONMOB), Fermi model, a parallel electric field dependent model (FLDMOB), recombination models (Shockley-read-hall, AUGER), incomplete ionization model (INCOMPLETE) and energy band narrowing model (BGN) [25]. The minority carrier lifetimes in the N-buffer and N-drift regions are set as 0.1 μs and 1.0 μs, respectively [26].

The main fabrication steps of the CTH-IGBT structure are given in Fig. 2 [27]. In the process of fabricating the device, it should be noted that the gate oxide layer is thermally grown under dry oxygen conditions in order to avoid the problem of insufficient oxide layer thickness at the bottom of trench under nominal thermal oxidation conditions [28]. Due to the small diffusion rate of impurity carriers in the SiC material, high-energy ion implantation is the only way to achieve high-quality, highly doped SiC [29], [30]. Additionally, in the device fabrication process, aluminum (Al) ion implantation [31]–[33] is used to form p-SiC. Although Al ion implantation can cause significant lattice damage, this can be mitigated by closely controlling the annealing and implantation conditions [34]. Furthermore, because the hardness of the SiC material is relatively large, it is very difficult to etch. We can use Ni as a mask and perform an inductively coupled plasma (ICP) etching containing SF_6/O_2 gas mixtures as effective etchants [35]. At the same time, we must pay close attention to the formation of micro-trenches during the etching process, which can cause the electric field concentration effect, thereby reducing the breakdown voltage of the device [35], [36].

III. SIMULATION RESULTS AND DISCUSSION

Fig. 3 shows the breakdown characteristic curves (V_{GE} = 0 V) of the C-IGBT, CT-IGBT and CTH-IGBT, respectively.

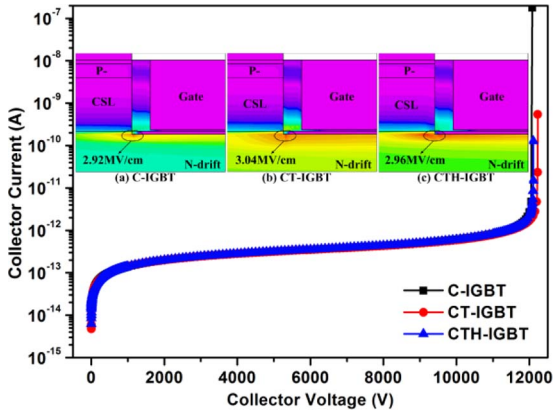

FIGURE 3. Breakdown characteristic curves and critical electric field distributions of (a) C-IGBT, (b) CT-IGBT and (c) CTH-IGBT.

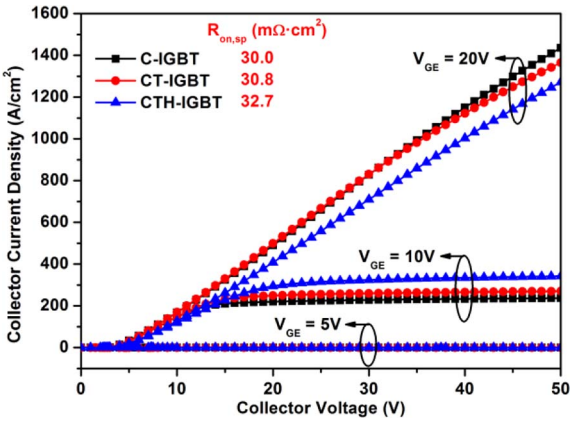

FIGURE 4. Forward I-V characteristics of (a) C-IGBT, (b) CT-IGBT and (c) CTH-IGBT.

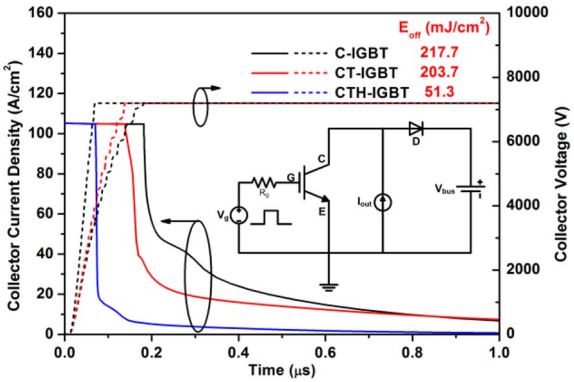

FIGURE 5. Turn-off characteristic curves of (a) C-IGBT, (b) CT-IGBT and (c) CTH-IGBT and test circuit schematic (inset).

We can see that the three devices can reach its avalanche breakdown voltage at about 12 kV when the gate and emitter contacts are connected to ground. At this time, the 2-D critical electric field distributions in these structures are given in the inset. It can be seen that when the devices undergo its avalanche breakdown voltage, the internal electric field peaks all appear at the corner of P+shielding region below the trench gate (the trench gate device is common in breakdown under the corner of the trench). The values of electric field peak for the C-IGBT, CT-IGBT and CTH-IGBT are 2.92 MV/cm, 3.04 MV/cm and 2.96 MV/cm, respectively, which approach the maximum 4H-SiC electric field strength of 3.0 MV/cm.

Fig. 4 illustrates the $I-V$ characteristics of the C-IGBT, CT-IGBT and CTH-IGBT. As can be seen from this figure, the specific ON-resistance ($R_{on,sp}$) of the C-IGBT, CT-IGBT and CTH-IGBT are estimated to be 30.0, 30.8 and 32.7 mΩ·cm^2 (V_{GE} = 20 V and V_{CE} = 20 V). As a result, $R_{on,sp}$ of the CTH-IGBT decreases slightly than that of the C-IGBT and CT-IGBT. The figure of merit (FOM = $V_{BR}^2/R_{on,sp}$) is used to indicate the tradeoff relationship between breakdown voltage and ON-resistance, and it can be calculated to 4.80, 4.77 and 4.40 kV^2/mΩ·cm^2 for the three structures, respectively.

Since the device stores a large number of minority carriers in the drift region during forward conduction process, the ON-resistance is usually very small, but this is very disadvantageous for the turn-off process of IGBT structure. When the device is turned off, the carriers stored in the drift region form a large tail current, which can extend the turn-off time of the device and increases the power loss during turn-off. In this simulation, the test circuit used to compare the shutdown performance of the C-IGBT, CT-IGBT and CTH-IGBT is shown in Fig. 5. The clamped inductive load is modeled by a constant current source ($I_{out} = 2.1 \times 10^{-6}$ A) and the bus voltage (V_{bus}) is set to 60% of the breakdown voltage. A gate voltage changing from 20 V to -5 V, with a frequency of 5 kHz and a 50% duty cycle, is introduced to control the turn-on and turn-off of the device. The simulated device's area is set as 2.1×10^{-8} cm^2, making the current density of 100 A/cm^2.

The turn-off characteristic curves of the C-IGBT, CT-IGBT and CTH-IGBT are presented in Fig. 5. The E_{off} of the C-IGBT, CT-IGBT and CTH-IGBT are calculated to be 217.7, 203.7 and 51.3 mJ/cm^2, respectively. The E_{off} of the proposed CTH-IGBT structure is 76.4% lower compared to that of the conventional structure, which is mainly due to the introduction of the p-polySi/p-SiC heterojunction on the collector side. In the conventional structure, the carriers stored in the drift region can only disappear by conventional recombination process. However, the proposed structure provides a more effective conduction path for the leakage of carriers. From the previous work on the improving of collector region, Si IGBT can demonstrate much lower E_{off} as shown in Table 2 [37], [38]. We can also see that, the 12 kV proposed CTH-IGBT can represent a comparative E_{off} performance compared with the 5.5 kV SiC SJ-IGBT [39]. Furthermore, the CTH-IGBT can demonstrate a significantly decrease in E_{off} in comparison with the other structures [39]–[42].

As can be seen from Fig. 6, the turn-off current of CTH-IGBT drops earlier and shows almost no current tail compared with the other two structures. So, a shorter turn-off time (T_{off}) of 0.12 μs is obtained, which can be decreased by

TABLE 2. Turn-off loss comparison with different type of devices.

Device	Reference	BV (kV)	E_{off} (mJ/cm^2)
CTH-IGBT	in this paper	12	51.3
CT IGBT (Si)	[37]	1.2	~7.5
SDC-IGBT (Si)	[38]	1.2	14.0
SJ-IGBT	[39]	5.5	>60.0
n-p-n-TIGBT	[40]	15	153.8
H-IGBT	[41]	15	152.3
DCS-IGBT	[42]	~20	>200.0

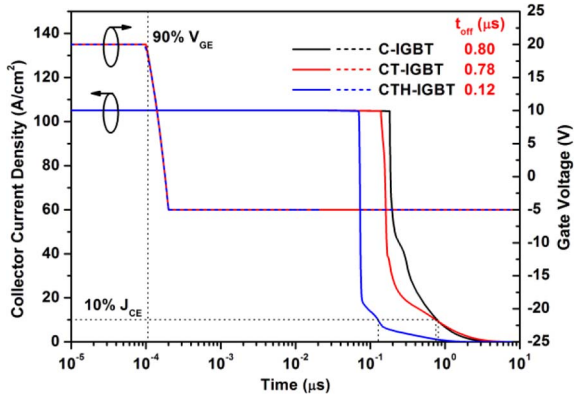

FIGURE 6. Turn-off current and voltage waveforms of (a) C-IGBT, (b) CT-IGBT and (c) CTH-IGBT.

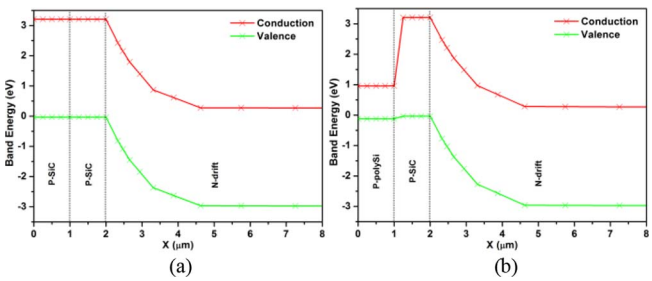

FIGURE 7. Energy band diagram comparison for the (a) CT-IGBT and (b) CTH-IGBT device in thermal equilibrium.

85.0% in comparison with that of C-IGBT ($T_{off} = 0.80$ μs). The main difference is because the carriers can now not only disappear by the process of recombination, but also flow into the collector through the low energy barrier region on the heterojunction side. The low energy band barrier region can be shown in Fig. 7 (cut line from AA' as shown in Fig. 1). As a result, the heterojunction portion of the CTH-IGBT can be more conducive to discharge the electrons during the device shutdown process.

Fig. 8(a) shows the distribution of the electron concentration and the carrier recombination rate on the collector side during voltage rise process (cut line from BB' as shown in Fig. 1). We can see that, for CTH-IGBT, the electron concentration is lower than that across the collector side of the C-IGBT and CT-IGBT. This is mainly because the

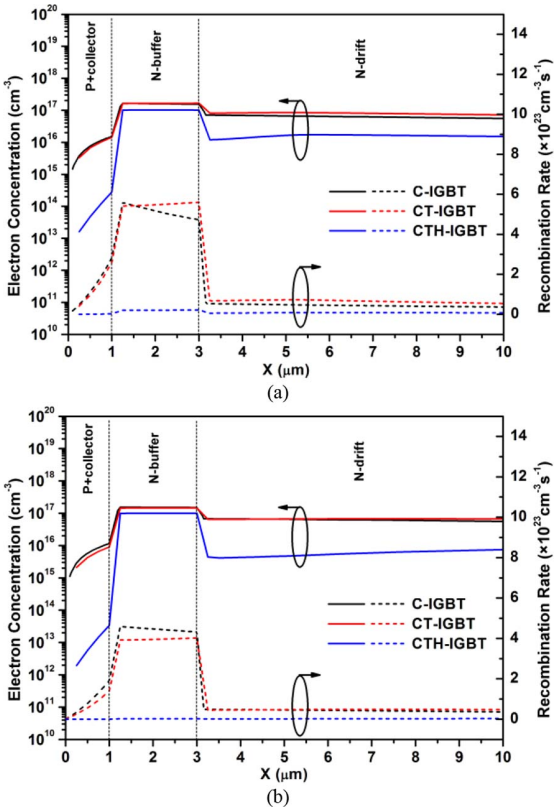

FIGURE 8. Electron concentration and carrier recombination rate on the collector side during (a) voltage rise phase at $t = 53$ ns and (b) current fall phase at $t = 200$ ns.

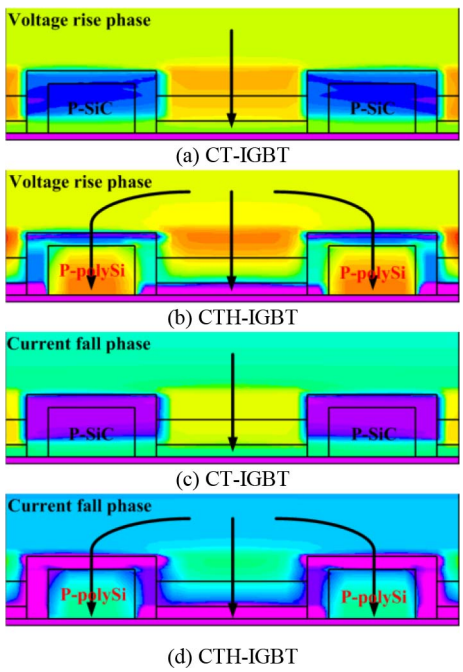

FIGURE 9. Simulated electron current paths during voltage rise phase at $t = 53$ ns and current fall phase at $t = 200$ ns.

heterojunction in trench collector can provide a very available conduction path to remove the injection electron. As a result, a very low electron concentration in CTH-IGBT

leads to a significant decrease in carrier recombination rate compared with the other two structures. For comparing the turn-off process during current fall phase, the electron concentration and carrier recombination rate of the structures are given at $t = 200$ ns in Fig. 8(b). It can be seen that very similar curve distributions are obtained in comparison with Fig. 8(a). Because of much lower electron concentration storing in CTH-IGBT durning current fall phase, T_{off} can be significantly improved compared with the other two structures.

The simulated electron current paths during turn-off process for the CT-IGBT and proposed CTH-IGBT are shown in Fig. 9. We can see that a prominent electron current path is formed in the heterojunction region between the n-drift and collector during turn-off process. Combined with the shallow electron potential well formed in the heterojunction region of the CTH-IGBT (as shown in Fig. 7), the formed electron current path can significantly accelerate the electron extraction in the drift region.

IV. CONCLUSION

We presented a CTH-IGBT with a p-polySi/p-SiC trench heterojunction on the backside of the device, and compared with the electrical characteristics of the C-IGBT and CT-IGBT using the Silvaco ATLAS simulation software. The simulation results verify excellent performance characteristics of the proposed structure. Under the premise of a constant breakdown voltage, the heterojunction can accelerate the extraction of electrons during turn-off process without affecting much the forward $I-V$ characteristic. In the end, the turn-off loss and turn-off time of the proposed device can be improved by 76.4% and 85.0% in comparison with that of the C-IGBT, respectively.

REFERENCES

[1] S. Chowdhury and T. P. Chow, "Performance tradeoffs for ultra-high voltage (15 kV to 25 kV) 4H-SiC n-channel and p-channel IGBTs," in *Proc. Int. Symp. Power Semicond. Devices ICs (ISPSD)*, Prague, Czech, Jun. 2016, pp. 75–78, doi: 10.1109/ISPSD.2016.7520781.

[2] X. L. Tian *et al.*, "Simulation study for the structural cell design optimization of 15kV SiC p-channel IGBTs," *Mater. Sci. Forum*, vol. 963, pp. 666–669, Jul. 2019, doi: 10.4028/www.scientific.net/MSF.963.666.

[3] K. Fukuda, "Development of ultrahigh-voltage SiC devices," *IEEE Trans. Electron Devices*, vol. 62, no. 2, pp. 396–404, Feb. 2015, doi: 10.1109/TED.2014.2357812.

[4] H. Andreas, H. Thomas, and E. Achim, "Analytical model for the influence of the gate-voltage on the forward conduction properties of the body-diode in SiC-MOSFETs," *Mater. Sci. Forum*, vol. 924, pp. 901–904, Jun. 2018, doi: 10.4028/www.scientific.net/msf.924.901.

[5] X. Li *et al.*, "Impact of termination region on switching loss for SiC MOSFET," *IEEE Trans. Electron Devices*, vol. 66, no. 2, pp. 1026–1031, Feb. 2019, doi: 10.1109/TED.2018.2888995.

[6] L. Sun, B. Duan, X. Yang, Y. Wang, and Y. Yang, "Analysis of the novel Si/SiC heterojunction IGBT characteristics by TCAD simulation & z.star," *Superlatt. Microstruct.*, vol. 122, pp. 1–4, Oct. 2018, doi: 10.1016/j.spmi.2018.06.031.

[7] S. H. Ryu *et al.*, "Ultra high voltage (>12 kV), high performance 4H-SiC IGBTs," in *Proc. IEEE Int. Symp. Power Semicond. Devices ICs*, 2012, pp. 1–6, doi: 10.1109/ISPSD.2012.6229072.

[8] X. Wang and J. A. Cooper, "High-voltage n-channel IGBTs on free-standing 4H-SiC epilayers," *IEEE Trans. Electron Devices*, vol. 57, no. 2, pp. 511–515, Feb. 2010, doi: 10.1109/ted.2009.2037379.

[9] Y. Yonezawa, T. Mizushima, and K. Takenaka, "Device performance and switching characteristics of 16 kV ultrahigh-voltage SiC flip-type n-channel IE-IGBTs," *Mater. Sci. Forum*, vols. 821–823, pp. 842–846, Jun. 2015, doi: 10.4028/www.scientific.net/MSF.821-823.842.

[10] D. Navarro, I. Pesic, Y. Morikawa, Y. Furui, and M. Miura-Mattauch, "Investigation of 4H-SiC IGBT turn-off performance for achieving low power loss," in *Proc. Int. Conf. Solid-State Devices Mater.*, 2015, pp. 502–503, doi: 10.7567/SSDM.2015.PS-14-9.

[11] Y. Kagawa, N. Fujiwara, and K. Sugawara, "4H-SiC trench MOSFET with bottom oxide protection," *Mater. Sci. Forum*, vols. 778–780, pp. 919–922, Feb. 2014, doi: 10.4028/www.scientific.net/MSF.778-780.919.

[12] Q. Zhang *et al.*, "12-kV p-channel IGBTs with low on-resistance in 4H-SiC," *IEEE Electron Device Lett.*, vol. 29, no. 9, pp. 1027–1029, Aug. 2008, doi: 10.1109/LED.2008.2001739.

[13] N. Watanabe, H. Yoshimoto, and A. Shima, "Impact of cell layout and device structure on on-voltage reduction of 6.5-kV n-channel SiC IGBTs," *Mater. Sci. Forum*, vol. 924, pp. 637–640, Jun. 2018, doi: 10.4028/www.scientific.net/msf.924.637.

[14] V. Naidu and S. Kotamraju, "Improved switching characteristics obtained by using high-k dielectric layers in 4H-SiC IGBT: Physics-based simulation," *Mater. Sci. Forum*, vol. 897, p. 4, May 2017, doi: 10.4028/www.scientific.net/MSF.897.571.

[15] S. H. Ryu, C. Capelll, and C. Jonas, "An analysis of forward conduction characteristics of ultra high voltage 4H-SiC N-IGBTs," *Mater. Sci. Forum*, vol. 858, pp. 945–948, May 2016, doi: 10.4028/www.scientific.net/MSF.858.945.

[16] N. Watanabe, H. Yoshimoto, and A. Shima, "6.5 kV n-channel 4H-SiC IGBT with low switching loss achieved by extremely thin drift layer," *Mater. Sci. Forum*, vol. 858, pp. 939–944, May 2016, doi: 10.4028/www.scientific.net/MSF.858.939.

[17] S. Chowdhury, C. W. Hitchcock, and Z. Stum, "Operating principles, design considerations, and experimental characteristics of high-voltage 4H-SiC bidirectional IGBTs," *IEEE Trans. Electron Devices*, vol. 64, no. 3, pp. 888–896, Mar. 2017, doi: 10.1109/ted.2016.2631241.

[18] J. P. Henning, K. J. Schoen, and M. R. Melloch, "Electrical characteristics of rectifying polycrystalline silicon/silicon carbide heterojunction," *J. Electron. Mater.*, vol. 27, no. 4, pp. 296–299, 1998, doi: 10.1007/s11664-998-0403-x.

[19] T. Kudoh and T. Asano, "Si/SiGe heterojunction collector for low loss operation of trench IGBT," *Appl. Surface Sci.*, vol. 224, no. 1, pp. 399–404, 2004, doi: 10.1016/j.apsusc.2003.08.096.

[20] J. Liang, S. Nishida, and T. Hayashi, "Effects of interface state charges on the electrical properties of Si/SiC heterojunctions," *Appl. Phys. Lett.*, vol. 105, no. 15, 2014, Art. no. 151607, doi: 10.1063/1.4898674.

[21] M. Nawaz and F. Chimento, "On the assessment of temperature dependence of 10-20kV 4H-SiC IGBTs using TCAD," *Mater. Sci. Forum*, vols. 740–742, pp. 1085–1088, Jan. 2013, doi: 10.4028/www.scientific.net/MSF.740-742.1085.

[22] B. Buono *et al.*, "Modeling and characterization of current gain versus temperature in 4H-SiC power BJTs," *IEEE Trans. Electron Devices*, vol. 57, no. 3, pp. 704–711, Mar. 2010, doi: 10.1109/ted.2009.2039099.

[23] M. K. Das, J. Zhang, R. Callanan, and C. Capell, "A 13 kV 4H-SiC n-channel IGBT with low rdiff, on and fast switching," *Mater. Sci. Forum*, vols. 600–603, pp. 1183–1186, Sep. 2009, doi: 10.4028/www.scientific.net/MSF.600-603.1183.

[24] M. Nawaz, "On the assessment of few design proposals for 4H-SiC BJTs," *Microelectron. J.*, vol. 41, no. 12, pp. 801–808, 2010, doi: 10.1016/j.mejo.2010.06.016.

[25] M. Usman and M. Nawaz, "Device design assessment of 4H-SiC n-IGBT-A simulation study," *Solid-State Electron.*, vol. 92, no. 5, pp. 5–11, 2014, doi: 10.1016/j.sse.2013.10.019.

[26] X. Li *et al.*, "A SiC power MOSFET loss model suitable for high-frequency applications," *IEEE Trans. Ind. Electron.*, vol. 64, no. 10, pp. 8268–8276, Oct. 2017, doi: 10.1109/TIE.2017.2703910.

[27] A. O. Konstantinov, Q. Wahab, and N. Nordell, "Ionization rates and critical fields in 4H silicon carbide," *Appl. Phys. Lett.*, vol. 71, no. 1, pp. 90–92, 1997, doi: 10.1063/1.119478.

[28] K. Kawahara, J. Suda, and T. Kimoto, "Analytical model for reduction of deep levels in SiC by thermal oxidation," *J. Appl. Phys.*, vol. 111, no. 5, pp. 199–204, 2012, doi: 10.1063/1.3692766.

[29] T. Kimoto, K. Kawahara, and H. Niwa, "Ion implantation technology in SiC for power device applications," in *Proc. Int. Workshop Junction Technol.*, 2014, pp. 1–6, doi: 10.1109/IWJT.2014.6842018.
[30] T. Kimoto *et al.*, "Ion implantation technology in SiC for high-voltage/high-temperature devices," in *Proc. IEEE 16th Int. Workshop Junction Technol. (IWJT)*, 2016, pp. 9965–9970, doi: 10.1109/iwjt.2016.7486673.
[31] C. A. Fisher, R. Esteve, and S. Doering, "An electrical and physical study of crystal damage in high-dose Al- and N-implanted 4H-SiC," *Mater. Sci. Forum*, vol. 897, pp. 411–414, May 2017, doi: 10.4028/www.scientific.net/MSF.897.411.
[32] X. Zhong, B. Wang, J. Wang, and K. Sheng, "Experimental demonstration and analysis of a 1.35-kV 0.92-mΩcm^2 SiC superjunction schottky diode," *IEEE Trans. Electron Devices*, vol. 65, no. 4, pp. 1458–1465, Apr. 2018, doi: 10.1109/ted.2018.2809475.
[33] C.-Y. Lee *et al.*, "A novel 4H-SiC trench MOS barrier schottky rectifier fabricated by a two-mask process," in *Proc. 25th Int. Symp. Power Semicond. Devices ICs (ISPSD)*, 2013, pp. 171–174, doi: 10.1109/ISPSD.2013.6694473.
[34] Y. Kawada *et al.*, "Shape control and roughness reduction of SiC trenches by high-temperature annealing," *Jpn J. Appl. Phys.*, vol. 48, Nov. 2009, Art. no. 116508, doi: 10.1143/JJAP.48.116508.
[35] L. E. Luna *et al.*, " Deep reactive ion etching of 4H-SiC via cyclic SF_6/O_2 segments," *J. Micromechan. Microeng.*, vol. 27, no. 9, pp. 1–12, 2017, doi: 10.1088/1361-6439/aa7c68.
[36] J. J. Wang *et al.*, "ICP etching of SiC," *Solid-State Electron.*, vol. 42, no. 12, pp. 2283–2288, 1998. [Online]. Available: https://doi.org/10.1016/S0038-1101(98)00226-3
[37] M. Jiang, X. Yin, Z. Shuai, J. Wang, and Z. J. Shen, "An insulated-gate bipolar transistor with a collector trench electron extraction channel," *IEEE Electron Device Lett.*, vol. 36, no. 9, pp. 935–937, Sep. 2015, doi: 10.1109/LED.2015.2462807.
[38] M. Vaidya, A. Naugarhiya, and S. Verma, "Trench IGBT with stepped doped collector for low energy loss," *Semicond. Sci. Technol.*, vol. 35, no. 2, Jan. 2020, Art. no. 025015, doi: 10.1088/1361-6641/ab6106.
[39] Z. Shen *et al.*, "Optimized P-emitter doping for switching-off loss of superjunction 4H-SiC IGBTs," in *Proc. 13th China Int. Forum Solid-State Light. Int. Forum Wide Bandgap Semicond. China (SSLChina:IFWS)*, 2016, pp. 1–5, doi: 10.1109/IFWS.2016.7803742.
[40] Y. Liu, Y. Wang, Y. Hao, C. Yu, and F. Cao, "4H-SiC trench IGBT with back-side n-p-n collector for low turn-OFF loss," *IEEE Trans. Electron Devices*, vol. 64, no. 2, pp. 488–493, Feb. 2017, doi: 10.1109/TED.2016.2639548.
[41] H.-K. Mao, Y. Wang, X. Wu, and F.-W. Su, "Simulation study of 4H-SiC trench insulated gate bipolar transistor with low turn-off loss," *Micromachines*, vol. 10, no. 12, p. 815, 2019.
[42] J. Wei *et al.*, "SiC trench IGBT with diode-clamped p-shield for oxide protection and enhanced conductivity modulation," in *Proc. IEEE 30th Int. Symp. Power Semicond. Devices ICs (ISPSD)*, Chicago, IL, USA, 2018, pp. 411–414, doi: 10.1109/ISPSD.2018.8393690.